frontiers | Frontiers in Chemical Engineering

TYPE Original Research
PUBLISHED 01 December 2025
DOI 10.3389/fceng.2025.1648187

OPEN ACCESS

EDITED BY
Kavitha S,
Karpagam Academy of Higher Education, India

REVIEWED BY
Sankar Chakma,
Indian Institute of Science Education and Research, Bhopal, India
Elnaz Sohani,
University of Nottingham, United Kingdom
Narendra Sadhwani,
Thermo Fisher Scientific, United States

*CORRESPONDENCE
David Antonio Buentello-Montoya,
david.buentello@tec.mx

RECEIVED 16 June 2025
REVISED 17 October 2025
ACCEPTED 31 October 2025
PUBLISHED 01 December 2025

CITATION
Maytorena-Soria VM, Buentello-Montoya DA and Aldana H (2025) Valorization of agricultural waste biomass via solar-driven gasification in regions with high solar resources: the case of Mexico.
Front. Chem. Eng. 7:1648187.
doi: 10.3389/fceng.2025.1648187

Valorization of agricultural waste biomass via solar-driven gasification in regions with high solar resources: the case of Mexico

Victor Manuel Maytorena-Soria[1], David Antonio Buentello-Montoya[2]* and Hugo Aldana[3]

[1]Departamento de Ingeniería Química y Metalurgia, Universidad de Sonora, Hermosillo, Mexico, [2]Tecnologico de Monterrey, Escuela de Ingenieria y Ciencias, Jalisco, Mexico, [3]Tecnologico de Monterrey, Escuela de Ingenieria y Ciencias, Nuevo Leon, Mexico

Gasification is a technology that can produce high-value fuels and chemicals from waste biomass, with challenges mainly associated to energy required and scaling up. At the same time, solar-driven gasification can tackle the problems associated to the energy required by allothermal systems, but its feasibility requires not only technological maturation, but also a strategic location. This work analyses the potential of solar gasification in Mexico using thermodynamic simulations, based on the Gibb's Free Energy method, and geographical and demographic information. Results indicate that states with large waste biomass production (e.g., Sinaloa and Veracruz) are better suited for solar gasification than states with a large direct normal irradiance (e.g., Sonora), particularly when based on the H_2/CO ratio of the syngas. An index (Per capita Energy Self-sufficiency Index, PESI) was defined to establish a metric for the potential of different states for solar gasification, and it was found that several states (for example, Sinaloa with 480% and Sonora with 245%) can produce more energy from solar gasification than their *per capita* consumption.

KEYWORDS

solar gasification, biomass gasification, thermodynamic modelling, bioenergy, bioenergy in Mexico

1 Introduction

Gasification is a technology where feedstock (such as coal, biomass or plastic) is decomposed under a controlled oxidation atmosphere (usually air or steam) to produce a mixture of gases, composed of H_2, CO, CH_4 and CO_2, called syngas (Buentello-Montoya et al., 2023a). The decomposition of biomass during gasification is endothermic, that is, requires a source of energy to drive the reactions. Depending on the oxidizing atmosphere, gasification can be autothermal (with oxygen or even air), where the energy released during the combustion stage can drive the process, or allothermal (with steam or CO_2), which requires an external source of energy. Although syngas from steam gasification usually has better quality than air-produced syngas, steam gasification is limited by the energy required for steam production (Mousavi Rabeti et al., 2023; Nathan et al., 2017; Freda et al., 2022).

However, even with its limitations, gasification remains an attractive technology due to the versatility of syngas, since it has different applications (Rafati et al., 2017).

At the same time, solar energy is basically limitless and could supply more than enough power to satisfy society's needs (Maytorena and Buentello-Montoya, 2022). Concentrated solar power (CSP) uses irradiation coming from the sun to harness heat, which can be used for heat or electricity production (Maytorena and Buentello-Montoya, 2022); CSP technologies vary in applications, approaches and scales, depending on the purpose. Examples of CSP technologies are heliostat fields, dish Stirling and parabolic trough collectors (PTCs) (Loutzenhiser and Muroyama, 2017). CSP can be coupled with thermochemical biomass treatments like gasification (in what is called solar gasification) to tackle restrictive energy consumption. In solar gasification, radiation is harnessed directly by the feedstock (in direct heating processes) or by a heat transfer fluid (in indirect heating processes) (Nathan et al., 2017; Loutzenhiser and Muroyama, 2017; Maytorena and Buentello-Montoya, 2024; Abanades et al., 2021). Compared to conventional allothermal gasification, solar gasification is supplied of heat through concentrated solar power increasing the process cold gas efficiency and reducing the carbon footprint (Wieckert et al., 2013). However, when compared to other biomass conversion technologies such as pyrolysis or anaerobic digestion, solar gasification faces challenges in scalability, reactor design, the intermittency of solar energy and the resistance of the reactor materials. Pyrolysis and anaerobic digestion, for example, are commercially mature and easier to implement at small scales, but they typically yield lower-value products (for example, biogas with a relatively low energy density, in the case of anaerobic digestion (Pecchi and Baratieri, 2019)), require large energy inputs or extensive upgrading (Maytorena and Buentello-Montoya, 2024). Solar gasification offers the advantage of producing hydrogen-rich syngas with a reduced fossil energy footprint, but its technological maturity remains limited to pilot-scale demonstrations and can be circumstantial based on the availability of resources, leading to extensive research to increase the technology readiness level. Some experimental studies on solar gasification have been conducted worldwide, focusing on steam as the gasifying agent, followed by CO_2 and, to a lesser extent, air or oxygen, as found in Table 1, where a summary of recent studies found in Scopus-indexed databases is included.

Although solar power can be relatively reliable in every location worldwide, the climatological characteristics favor some geographical locations (Global Solar Atlas, 2020). A particular case is Mexico, where based in the Global Solar Atlas, the World Bank has reported that around 0.1% of the total area is enough to produce enough energy to satisfy its needs (Global Solar Atlas, 2020; World Bank, 2020). Moreover, Mexico generates more than 30,000 Mtons of organic waste per year, which can serve as a decentralized feedstock for energy production from gasification, tackling constraints associated to resource availability (Molina-Guerrero et al., 2020; Aldana et al., 2014).

This work addresses research gaps by presenting a nationwide assessment of the geographic potential of solar-driven gasification in Mexico, moving beyond reactor-scale demonstrations to whole region analysis based on a simulation model. Since the hydrodynamics and transport phenomena associated with gasification can be heavily dependent on the biomass physical properties, a complete Computational Fluid Dynamics study considering different biomasses with variable composition across a whole country is prohibitively complicated. Similarly, kinetic studies usually consider biomass "lumps" or model compounds, hence, results can become complicated to relate with varying and diverse biomass composition. Therefore, thermodynamic equilibrium modeling is combined with information on state-level biomass availability and solar resource data to identify regions in Mexico where solar gasification could provide meaningful energy contributions or support alternatives such as hydrogen-based chemical production. For the analysis, calculations were conducted using thermodynamic simulations based on an in-house-developed Python code. The reported information can be relevant for engineers, scientists and stakeholders in different countries with similar scenarios. The integrated approach presents the potential relevance of combined CSP and waste-to-energy technologies in countries with both high solar resources and significant agricultural waste streams.

To provide an insight into the potential of solar gasification when compared to the autothermal technology using air (that is, non-solar), results are presented under the same conditions considering (Buentello-Montoya et al., 2023a) air and (Mousavi Rabeti et al., 2023) steam as gasification agents. The structure of the work is as follows. After the introduction, the methodology is conferred, starting with a description of the model employed in the simulations, followed by the methodologies used to assess the performance of gasification and information on the input used on each state. The following section presents and discusses the results. In the results and discussion section, firstly, autothermal (non-solar) and allothermal gasification with steam are compared in terms of the heating value of the produced gas and process efficiency. Afterwards, results are presented by state where the potential of solar gasification is assessed based on aspects such as the solar energy received by the state and the average agricultural waste biomass composition, among others. Finally, the manuscript closes by presenting a summary and a series of conclusions from the findings.

2 Methodology

2.1 Description of the thermodynamic model

The model employed in the simulations is a thermodynamic equilibrium model which follows the Gibb's free energy minimization method as found in Equation 1 (Privat et al., 2016):

$$\Delta G = \min\left[\sum y_i g_i^0\right] \tag{1}$$

Where ΔG is the change in Gibbs' free energy, y_i are the moles of species i, and g_i^0 is the molar Gibbs' free energy of species i. The model is based on in-house developed Python code that simulates equilibrium, assuming an infinitely long residence time (suitable for downdraft and some fluidized bed gasifiers), constant temperature and pressure (Abanades et al., 2021). In every simulation, the

TABLE 1 Summary of experimental solar gasification studies reported between 2015 and 2025.

Gasification agent	Temperature range/power	Notes	Ref.
Steam and oxygen	>900 °C	Experimental molten salt solar gasifier	Hathaway and Davidson (2021)
Steam	150 kW_{th}	Fixed bed reactor, temperatures >1,200 °C	Wieckert et al. (2013)
Steam	3 kW_{th}	Residence time <5 s	Müller et al. (2017)
Steam	1 kW_{th}	Hybrid solar/autothermal gasifier	Muroyama et al. (2018)
Steam	700/1200W_{th}	Hybrid solar/autothermal gasifier, directly or indirectly heated	Curcio et al. (2021)
Steam	150 kW_{th}	Concentrated solar power tower	Wieckert et al. (2013)
Steam	7 kW_e	Biomasses with normally high moisture	Arribas et al. (2017)
Steam	1.5 kW_{th}	Conical spouted bed reactor	Boujjat et al. (2020)
Steam	2.2 kW	Indirectly heated fluidized bed for hydrogen production	Li et al. (2020)
CO_2	7.7 kW	Indirectly heated fluidized bed	Li et al. (2021)
CO_2	2.2 kW_{th}	Molten salt gasifier	Hathaway and Davidson (2017)
CO_2	>1,000 °C	Coal and coke gasification	Kodama et al. (2010)

TABLE 2 Overall Mean Absolute Error, calculated from results from the simulations and the experiments.

Species	RMSE
H_2	0.643
CO	0.449
CO_2	0.563
CH_4	0.245
Average	0.475

material and energy balances were solved to ensure accuracy, whereas transport phenomena were ignored. The model was validated against experimental data reported in literature; the feedstock composition, gasification agent and gasification temperature were replicated, and the simulation results were compared with the reported syngas composition in each case (Cho et al., 2014; Gai and Dong, 2012; Jayah et al., 2003; Kramb et al., 2014; Tuomi et al., 2015; Xiao et al., 2007; Fazil et al., 2022; Loha et al., 2011; Duan et al., 2014; Samani et al., 2024). The Root Mean Square Error (RMSE) was calculated by species and used as an indicator of the accuracy of the model. The RMSE was calculated with Equation 2:

$$RMSE = \frac{\sqrt{\sum (Y_i - X_i)^2}}{n} \quad (2)$$

Where Y_i is the mole flow of species i obtained from the simulations, X_i is the mole flow of species i reported in literature and n is the number of replicated experiments for a given species.

The average RMSE by species is presented in Table 2 (which serves to determine which species has the largest error), while Table 3 presents details on the simulated literature. The global average RMSE value is less than 5%, which indicates agreement and accuracy of the model when compared with similar models with MAEs ranging from less than 5% to more than 10% (Puig-Arnavat et al., 2010).

2.2 Material balance

The mass balances were solved at the gasification temperatures and considering the feedstock biomass compositions, to fulfill the minimization of the Gibbs' free energy (Privat et al., 2016). While gasification involves a number of reactions and stages (for example, drying, devolatilization, pyrolysis and reduction (Maytorena and Buentello-Montoya, 2024)), Gibb's free energy based models do not include full kinetics and instead use a single global reaction that accounts for all of the semi reactions, and provide accurate results for gasifiers with long residence times (such as downdraft and fluidized bed gasifier) (Privat et al., 2016).

The mass balance (Equation 3) involved solving the global reaction and finding the components fraction at the minimum Gibb's free energy, considering H_2, CO, CO_2, CH_4, H2O and a tar (C_6H_6) as the possible products:

$$CH_\alpha O_\beta + \gamma(O_2 + 3.76N_2) + \delta H_2O_{(g)} \longrightarrow x_1H_2 + x_2CO + x_3CO_2 + x_4CH_4 + x_5Tar + x_6H_2O + 3.76\gamma N_2 \quad (3)$$

Where α and β are normalized values based on the biomass ultimate analysis (and considering the subindex of carbon as 1), x_i is the mass fraction of the i species in the product, γ is the normalized injected air mass fraction and δ is the normalized injected steam mass fraction. In order to solve the global reaction, mass balance equations for carbon, hydrogen and oxygen were established, in addition to three equilibrium equations for the Water-Gas Shift (WGS) (Equation 4), methanation (Equation 5) and carbon gasification (Equation 6):

$$H_2O + CO \rightleftarrows H_2 + CO_2 \quad (4)$$

TABLE 3 Details on the literature simulated to validate the model, the reported syngas composition and the simulations retults.

Ref.	Gas	Feedstock composition (weight %)				Literature syngas composition (weight %)				Simulation syngas composition (weight %)			
		C	H	O	N	H_2	CO	CO_2	CH_4	H_2	CO	CO_2	CH_4
Tuomi et al. (2015)	Air	53.2	5.5	37.1	0.3	20.2	16.1	15.9	3.8	18.69	18.98	16.66	5.63
Gai and Dong (2012)	Air	43.83	5.95	45.01	0.97	6.91	11.35	20.37	1.84	9.89	14.73	21.47	5.41
Xiao et al. (2007)	Air	86.42	12.28	0	0.72	5	22	11	4.7	7.71	25.14	18.51	6.14
Cho et al. (2014)	Air	80.8	12.8	5.10	0.20	26.69	7.27	8.72	6.39	23.55	15.51	15.33	6.03
Fazil et al. (2022)	Air	42.38	5.24	35.41	1.78	10.76	14.79	18.11	1.35	9.49	18.18	21.19	4.58
Fazil et al. (2022)	Air	85.32	14.68	0	0	13.53	19.54	2.18	11.49	15.87	24.98	17.41	6.63
Duan et al. (2014)	Steam	64.53	3.75	7.00	0.96	59.8	25.4	14.7	0.1	40.58	30.12	13.43	3.57
Li et al. (2019)	Steam	41.61	5.45	50.70	1.64	33.27	34.97	24.7	7.06	26.64	35.31	23.22	5.19
Li et al. (2019)	Steam	41.67	5.42	52.33	0.03	38.42	36.1	19.3	6.18	29.08	36.98	18.98	4.57
Li et al. (2019)	Steam	48.93	6.22	42.16	0.92	39.1	43.14	11.3	6.46	29.88	36.55	25.66	6.17
Samani et al. (2024)	O_2/Steam	54.8	6.3	37.69	0.78	41.5	29.5	26.3	2.7	33.66	28.14	19.09	5.43

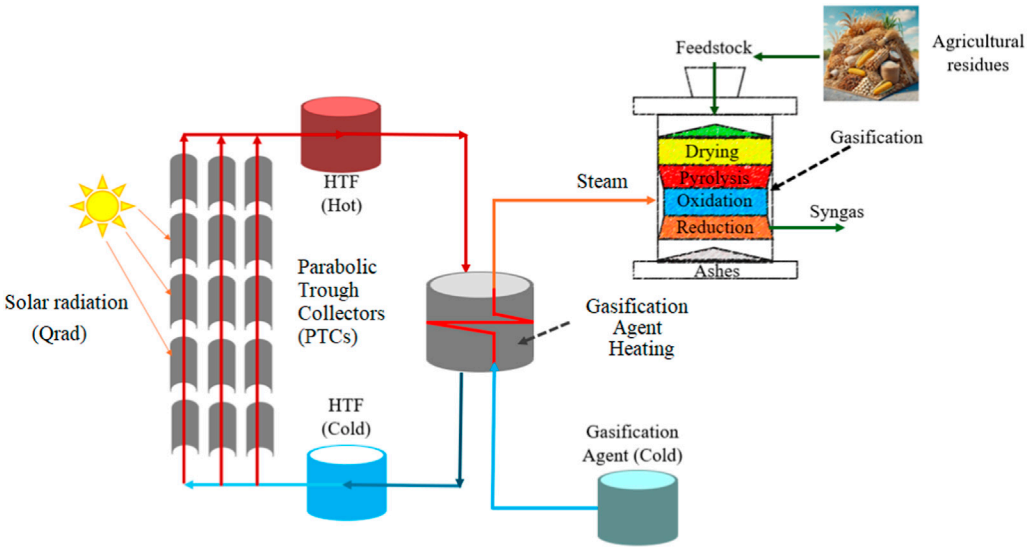

FIGURE 1
Schematic of the solar gasification reactor system emulated during the simulations. Heat is collected using Parabolic Trough Collectors and used to heat a heat transfer fluid, which is then used to generate steam for gasification.

$$C + 2H_2 \rightleftarrows CH_4 \quad (5)$$

$$C + H_2O \rightleftarrows H_2 + CO \quad (6)$$

The air mass was established as a function of the equivalence ratio, *ER*, calculated with Equation 7:

$$\beta = ER\left(1 + \frac{1}{12}\frac{H_{biomass}}{C_{biomass}} - \frac{3}{8}\frac{O_{biomass}}{C_{biomass}}\right) \quad (7)$$

The steam mass was calculated with Equation 8 from the steam-to-biomass ratio (SBR):

$$SBR = \frac{Y_{steam}}{Y_{biomass}} \quad (8)$$

Where Y_i are the mole flows of the species *i*.

Tar was assumed as C_6H_6 (benzene) and subsequently decomposed into C_7H_8 (toluene) and $C_{10}H_8$ (naphthalene) following the mechanism proposed in literature and involving Equations 9–15 (Jess, 1996; Norinaga et al., 2014; Frenklach, 2002):

$$C_6H_6 \rightleftarrows 3CH_2^* + 3C^* \quad (9)$$

$$C_6H_6 \rightleftarrows 3C_2H_2^* \quad (10)$$

$$C_6H_6 \rightleftarrows C_6H_5^* + H^* \quad (11)$$

$$C_6H_6 + CH_2^* \longrightarrow C_7H_8 \quad (12)$$

$$C_6H_5^* + C_2H_2^* \longrightarrow C_8H_7^* + H^* \quad (13)$$

TABLE 4 Average direct normal irradiation received per day by the states of Mexico (Global Solar Atlas, 2020).

#	State	Daily average DNI, kWh/m^2	Maximum theoretical temperature, °C	#	State	Daily average DNI, kWh/m^2	Maximum theoretical temperature, °C
1	Aguascalientes	6.89	704	14	Oaxaca	6.46	670
2	Chihuahua	7.54	757	15	Puebla	6.53	675
3	Ciudad de México	5.62	600	16	Querétaro	6.44	667
4	Durango	7.40	745	17	Quintana Roo	5.14	559
5	Guanajuato	6.54	676	18	San Luis Potosí	6.64	684
6	Guerrero	5.65	602	19	Sinaloa	6.28	654
7	Hidalgo	5.70	606	20	Sonora	7.49	752
8	Jalisco	6.31	657	21	Tabasco	4.48	502
9	México	5.72	608	22	Tamaulipas	5.41	582
10	Michoacán	5.67	604	23	Tlaxcala	6.36	661
11	Morelos	5.87	621	24	Veracruz	4.37	573
12	Nayarit	6.17	646	25	Yucatán	5.30	711
13	Nuevo León	5.26	570	26	Zacatecas	6.99	573

TABLE 5 Average ultimate composition from the agricultural waste in different states in Mexico, in weight percent.

#	State	C	H	O	N	S	#	State	C	H	O	N	S
1	Aguascalientes	47.83	6.33	44.96	0.74	0.07	14	Oaxaca	48.81	6.16	44.12	0.47	0.07
2	Chihuahua	49.12	7.53	41.36	1.13	0.04	15	Puebla	48.15	6.19	44.06	0.70	0.07
3	Ciudad de México	45.19	6.11	45.64	3.10	0.02	16	Querétaro	48.57	6.36	44.26	0.71	0.08
4	Durango	46.57	6.32	45.60	0.84	0.06	17	Quintana Roo	49.42	6.06	44.10	0.30	0.06
5	Guanajuato	48.68	6.25	44.01	0.62	0.09	18	San Luis Potosí	48.93	6.04	44.24	0.34	0.06
6	Guerrero	48.41	6.35	44.11	0.69	0.08	19	Sinaloa	48.04	6.30	44.25	0.77	0.07
7	Hidalgo	48.18	6.26	43.82	0.71	0.09	20	Sonora	48.14	6.39	44.00	0.94	0.07
8	Jalisco	48.49	6.22	43.55	0.55	0.07	21	Tabasco	49.45	6.11	44.00	0.34	0.07
9	México	48.26	6.33	43.87	0.80	0.08	22	Tamaulipas	49.40	6.19	43.58	0.45	0.08
10	Michoacán	48.74	6.30	43.87	0.63	0.08	23	Tlaxcala	48.17	6.34	44.07	0.72	0.09
11	Morelos	49.20	6.06	43.57	0.36	0.07	24	Veracruz	49.33	6.09	44.06	0.37	0.06
12	Nayarit	48.42	6.07	45.61	0.48	0.06	25	Yucatán	47.64	6.46	44.75	0.75	0.09
13	Nuevo León	46.76	6.16	44.26	1.67	0.06	26	Zacatecas	43.08	5.88	48.19	0.95	0.03

$$C_8H_7^* + C_2H_2^* \longrightarrow C_{10}H_9^* \quad (14)$$

$$C_{10}H_9^* \longrightarrow C_{10}H_8 + H^* \quad (15)$$

2.3 Energy balance

A parabolic trough collector was assumed as the employed technology to harness the solar radiation and fuel the reactions in each case, with a solar receiver Concentration Ratio (CR) of 100 (Sajjadnejad et al., 2020). The heat that was absorbed by the heat transfer fluid (HTF) was calculated with Equation 16:

$$Q_{Rad} = \eta_{Receiver} \cdot CR \cdot DNI \quad (16)$$

Where Q_{Rad} is the energy collected by the solar receiver and transferred to the HTF, DNI is Direct Normal Irradiation and $\eta_{Receiver}$ is the solar collector efficiency. Figure 1 portrays a schematic

TABLE 6 Base data for the cost analysis (Boujjat et al., 2021).

Concept	Value	Unit
Plant capacity (Bio_{base})	870	Ton_{dry}/day
Direct Capital Cost (DCI_{base})	360.31	million$ (2024)
Plant staff base (NO_{base})	54	Operators
Water consumption factor for the gasification process (WP_f)	0.66	$l/kg_{dry\text{-}biomass}$
Water consumption factor for mirrors cleaning (WC_f)	18	l/MWh
Electricity consumption factor (Ec_f)	0.17	$kWh/kg_{dry\text{-}biomass}$
Othe Variable Cost (OVC_{base})	11	million$/year (2024)

TABLE 7 Variable cost factors (considering 2024 prices).

Concept	Value	Unit	Reference
Operator salary	528.6	$/month	Ministry of Economy Secretaría de Economía (2025)
Electricity price	82.06	$/MWh	Secretaría de Energía SENER (2023)
Water price	2.24	$/m^3	Mexican Institute for Competitivenes (2023)
Biomass price	16.37	$/ton	El Sol de Hidalgo (2025)

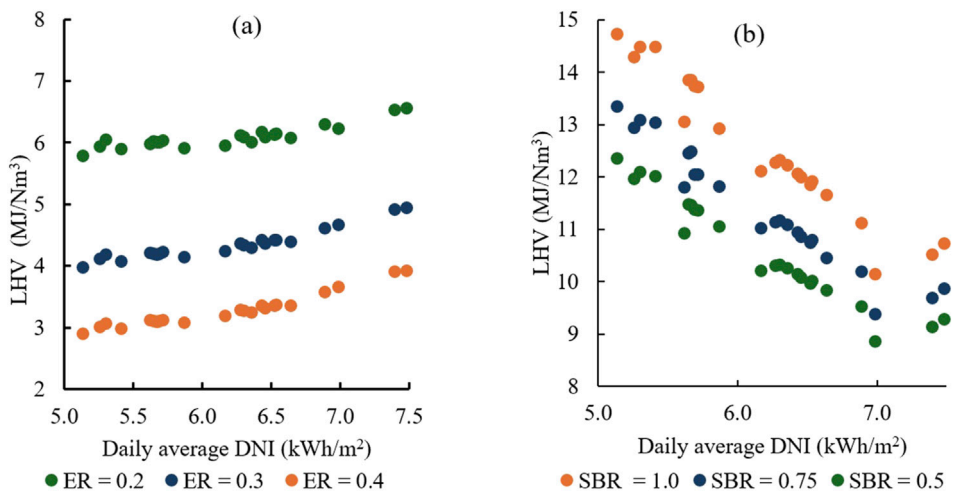

FIGURE 2
Effect of the DNI in the syngas LHV using **(a)** air and **(b)** steam as gasification agent.

of the simulated system. DNI is captured by PTCs and transferred to the HTF. The hot HTF is then used to heat the gasifying agent (air or steam), which is then used for gasification inside the reactor, producing the syngas stream.

It was assumed that the receiver has a constant efficiency of 80% (Maytorena and Buentello-Montoya, 2022). The *DNI* for every state were extracted from the Global Solar Atlas (Global Solar Atlas, 2020); the average daily flux for the different states, and the maximum theoretical temperature that can be reached by a black body with 100% efficiency under the studied conditions is portrayed in Table 4.

Since the used model assumes thermodynamic equilibrium, the achievable temperature by the HTF was calculated following Equation 17 (Stefan-Boltzmann's law):

$$Q_{Rad} = \varepsilon\sigma\left(T_{HTF}^4 - T_0^4\right) \tag{17}$$

Where ε is the collector's emissivity, σ is the Stefan-Boltzmann constant and T_0 and T_{HTF} are the ambient and HTF temperatures, respectively.

The temperature achievable by the reactants inside the gasifier was calculated with Equation 18:

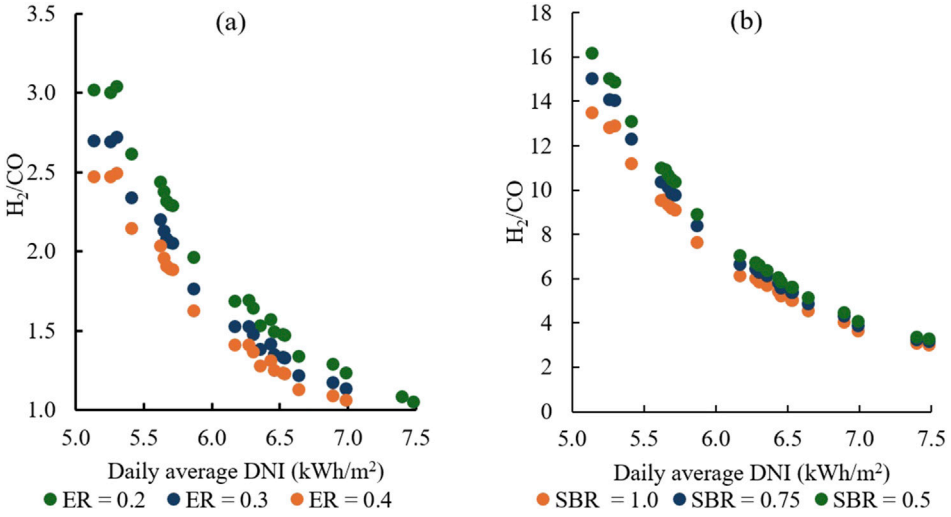

FIGURE 3
Effect of the DNI and gasification agent in the syngas H_2/CO ratio, where **(a)** corresponds to air and **(b)** to steam as agent, respectively.

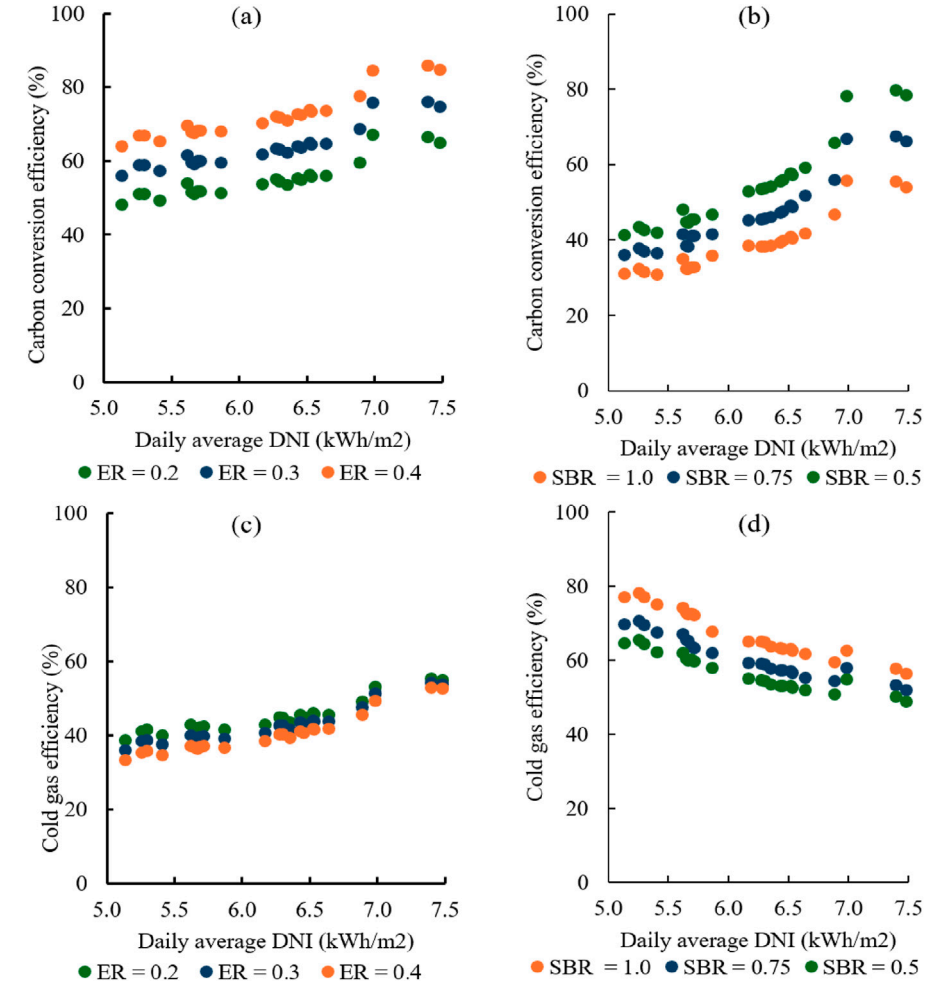

FIGURE 4
Effect of the DNI in the process CCE using air and steam as gasification agent. **(a)** CCE using different ERs (0.2, 0.3 and 0.4), **(b)** CCE using different SBRs (0.5, 0.75 and 1.0), **(c)** CGE using different ERs (0.2, 0.3 and 0.4) and **(d)** CGE using different SBRs (0.5, 0.75 and 1.0).

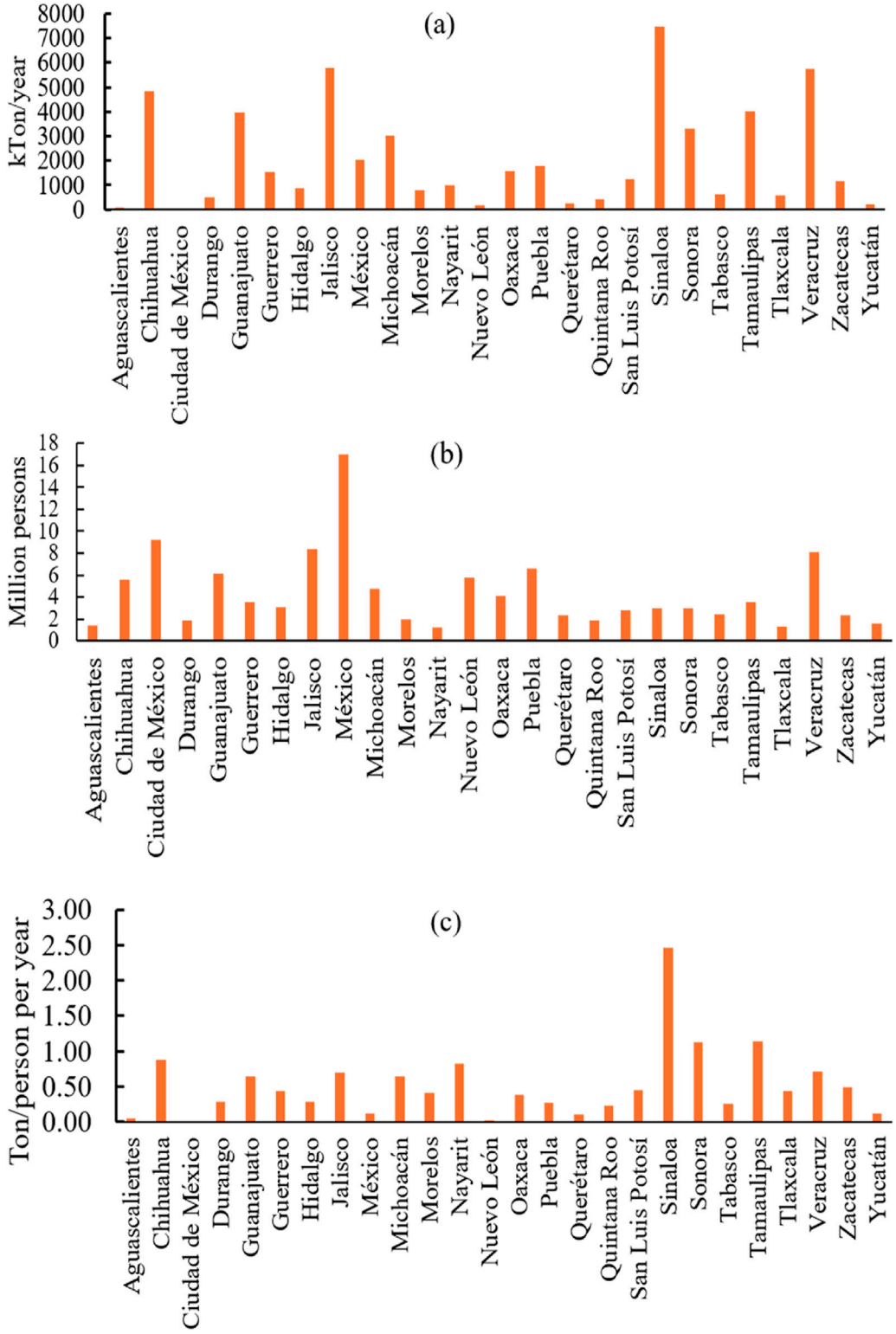

FIGURE 5
(Continued).

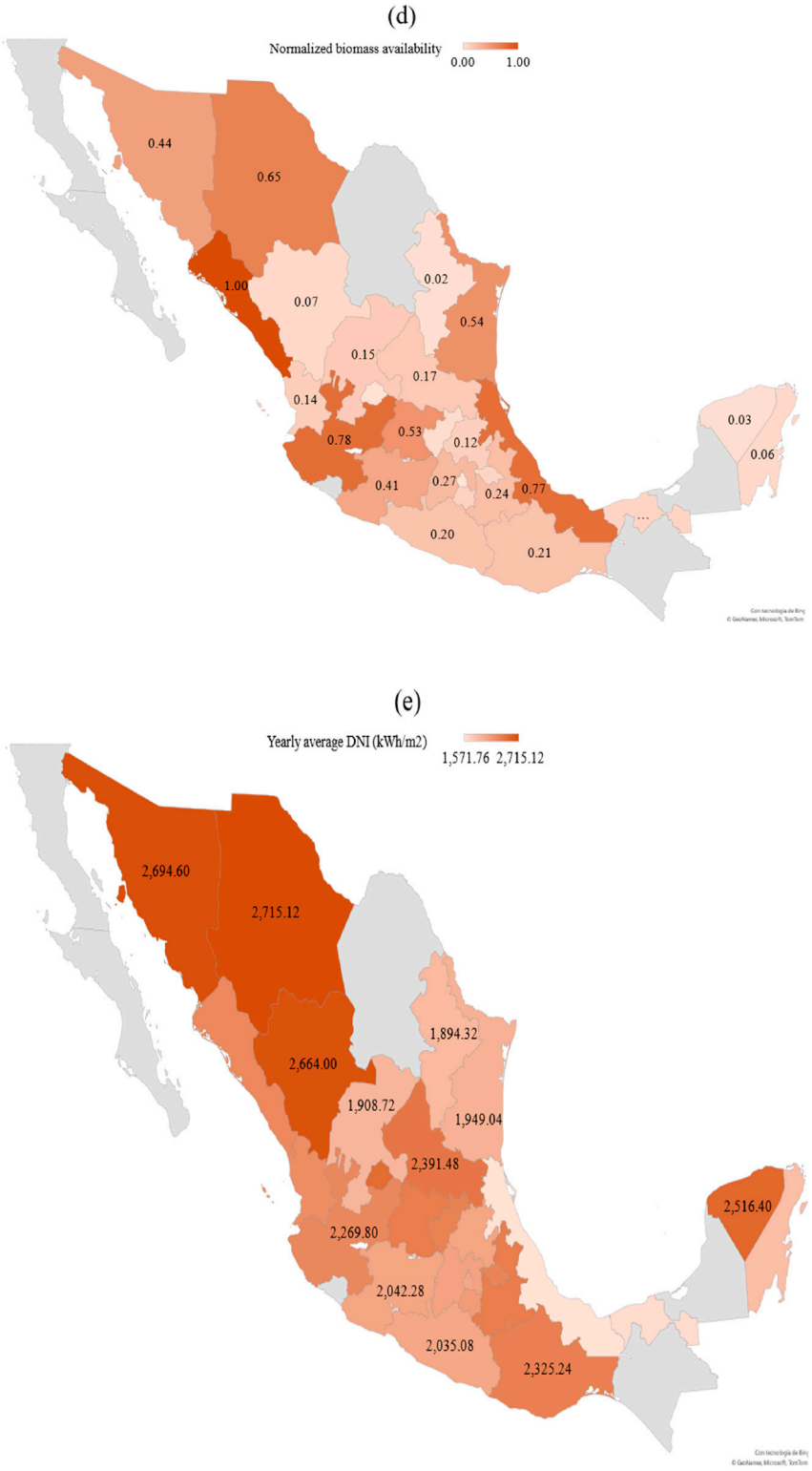

FIGURE 5
(Continued). Biomass availability and DNI by state, where **(a)** shows the waste biomass by state (in tons/year), **(b)** shows the waste biomass *per capita*, **(c)** shows a map of the normalized waste generation, **(d)** shows the normalized average biomass waste generation and **(e)** shows the average yearly DNI (in kWh/m^2) (Global Solar Atlas, 2020).

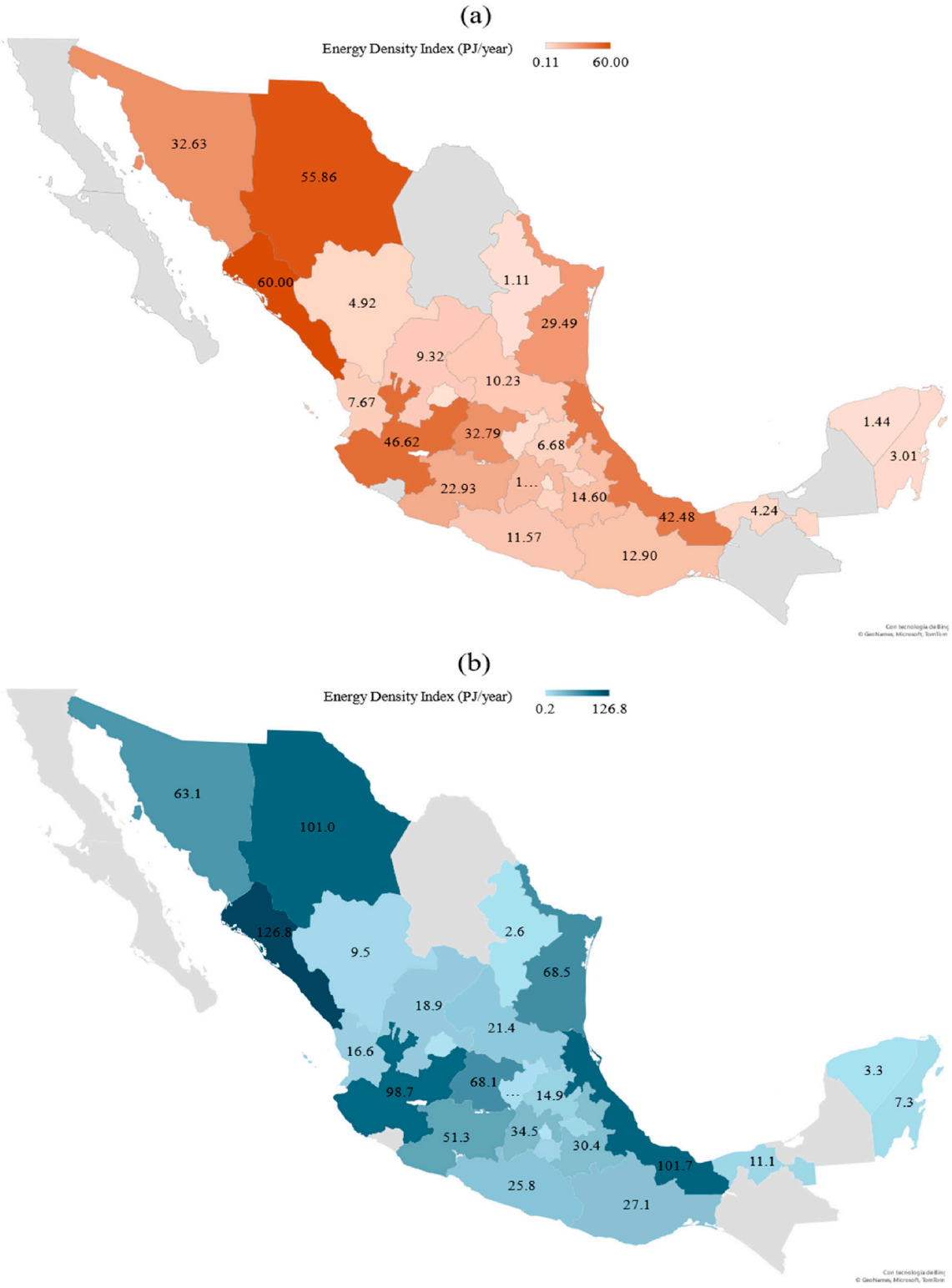

FIGURE 6
Energy Density Index in PJ/year, obtained with **(a)** air and **(b)** steam gasification.

10.3389/fceng.2025.1648187

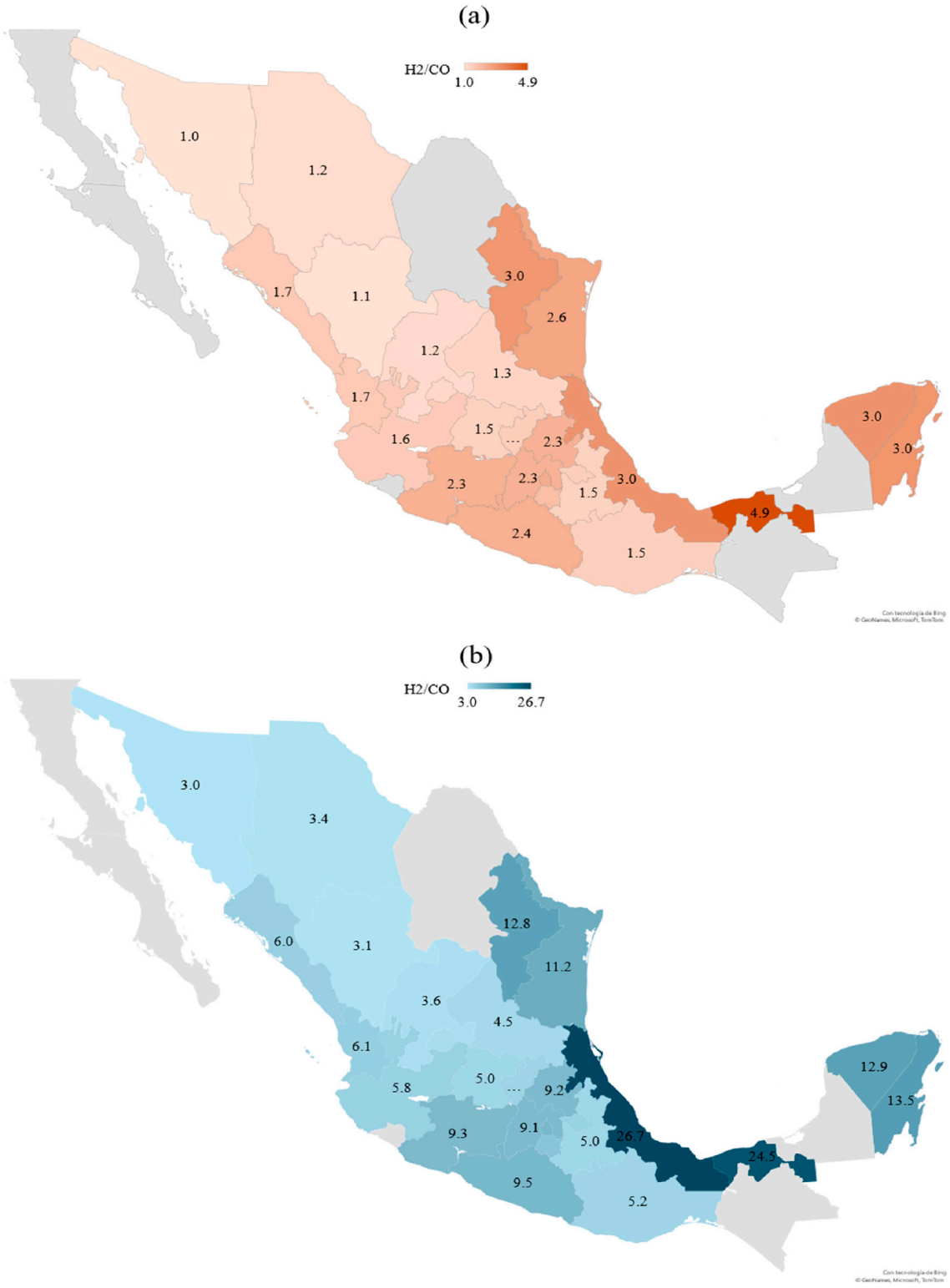

FIGURE 7
H_2/CO ratio by state. **(a)** Corresponds to air gasification and **(b)** to steam gasification.

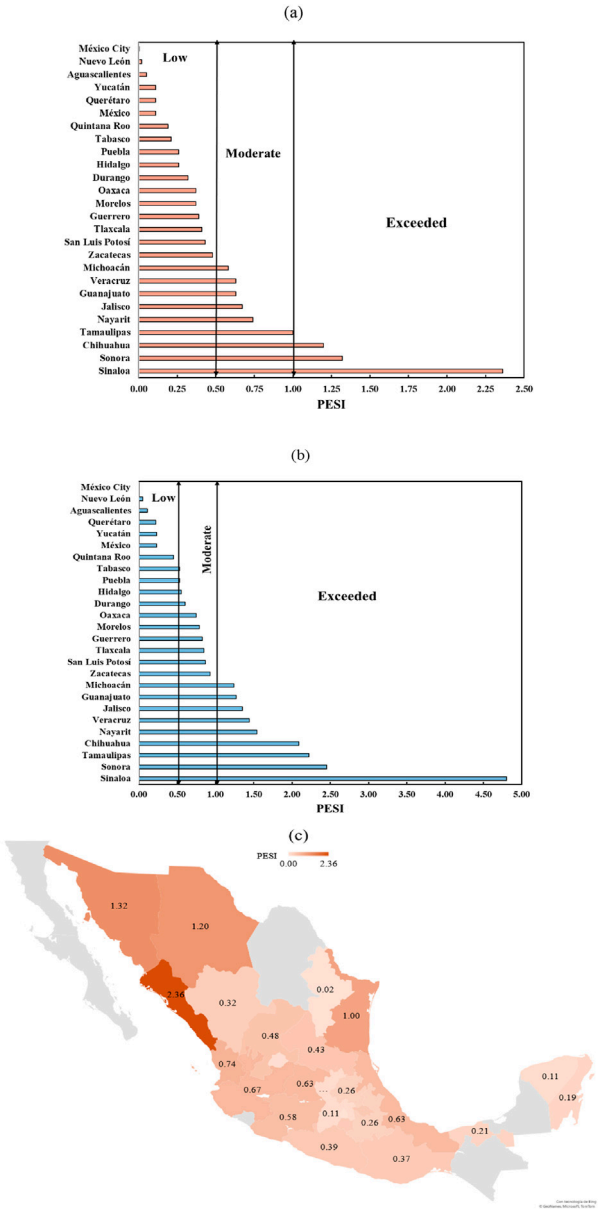

FIGURE 8
(Continued).

$$T_{gas} = T_0 + \eta_{HE}\frac{Q_{Rad}}{\sum C_{p,i} m_i} \quad (18)$$

Where η_{HE} is the heat exchanger efficiency and $C_{p,i}$ and m_i are the specific heat and masses of species i.

The enthalpy of reaction was calculated with Equation 19:

$$\Delta H_{Rxn} = \sum y_i \Delta h_i^0 \quad (19)$$

Where Δh_i^0 is the enthalpy of formation of species i. The heat of formation ($\Delta H^0_{Biomass}$) and Lower Heating Value of the fed waste biomass ($LHV_{Biomass}$, in MJ/kg) were calculated with Equations 20, 21:

$$\Delta H^0_{Biomass} = \Delta H^0_{CO_2} + \frac{\alpha}{2}\Delta H^0_{H_2O} + (12 + \alpha + 16\beta) LHV_{Biomass} \quad (20)$$

$$LHV_{Biomass} = 34.835 w_c + 93.87 w_H - 10.8 w_O + 6.28 w_N + 10.465 w_S \quad (21)$$

Where w_i is the mass fraction of species i, from the ultimate analysis of the processed biomass.

2.4 Gasification efficiency assessment

To assess the gasification process, different parameters were employed; a commonly used index is the Cold Gas Efficiency (CGE), which is defined as the ratio between the heating values of the syngas and the feedstock and was calculated with Equation 22:

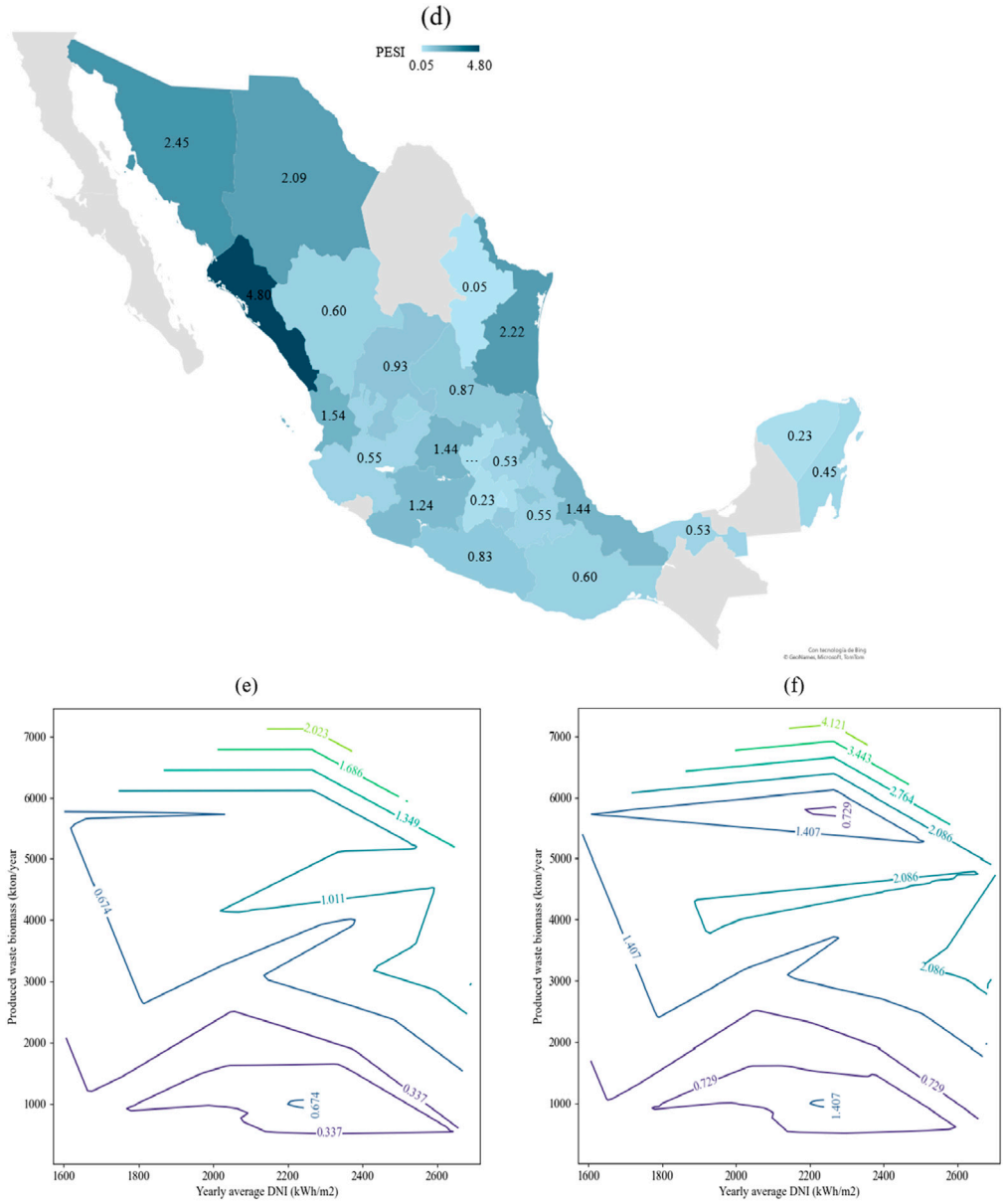

FIGURE 8
(Continued). Per capita Energy Self-sufficiency Index (PESI) by state, calculated using **(a)** air and **(b)** steam as gasification agent, maps of the PESI using **(c)** air and **(d)** steam, and **(e)** and **(f)** show the PESI as a function of the available waste biomass and DNI for air and steam, respectively.

$$CGE = \frac{LHV_{syngas}}{LHV_{Biomass}} \tag{22}$$

Where the LHV of the syngas (in MJ/Nm^3) is calculated with Equation 23 from its composition (Khartchenko and Kharchenko, 2014):

$$LHV_{syngas} = 4.18\left(2.57Y_{H_2} + 3.0Y_{CO} + 8.54Y_{CO_2} + 15.13Y_{CH_4}\right) \tag{23}$$

Additionally, the Carbon Conversion Efficiency (*CCE*) (Equation 24) was calculated as the ratio of carbon moles in the syngas and the carbon moles in the biomass (Khartchenko and Kharchenko, 2014):

$$CCE = \frac{Y_{CO} + Y_{CO_2} + Y_{CH_4}}{Y_{C,Biomass}} \tag{24}$$

2.5 Analysis of the potential of gasification in México

To determine the potential of gasification an analysis per state was performed. First, the availability of the biomass and the population of each state was determined. Then, an average availability *per capita* was estimated by dividing the total produced biomass ($m_{waste\ per\ year}$) by the population, as found in Equation 25:

$$Biomass\ per\ capita = \frac{m_{waste\ per\ year}}{population} \tag{25}$$

Based on the biomass availability and DNI, energy density index (EDI), which represents the maximum achievable energy to be produced via gasification with air or steam (using solar energy

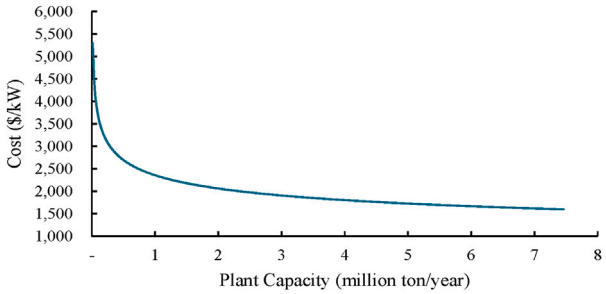

FIGURE 9
Unitary cost per capacity of power production (UCC_{state}).

as a source of energy was calculated). The EDI was calculated from the syngas LHV, and the available waste biomass (Equation 26):

$$EDI = LHV_{syngas} m_{waste\ per\ year} \tag{26}$$

Where $m_{waste\ per\ year}$ represents the yearly availability of waste per state. After that, considering the DNI and the composition of biomass per state a H_2/CO ratio was calculated, to determine the areas with larger potential for hydrogen or chemical production.

Finally, to assess how the energy demand per state compares to the energy production potential, the Per capita Energy Self-sufficiency Index (PESI) was defined. The PESI (Equation 27) describes the energy contents in the produced syngas associated to the *per capita* produced waste to the *per capita* consumed energy:

$$PESI = \frac{LHV_{Syngas} m_{waste\ per\ capita}}{E} \tag{27}$$

Where E is the consumed energy *per capita*, equaling 2,425 kWh, according to SENER (Mexico's federal energy secretariat) (Secretaría de Energía SENER, 2023); importantly, E accounts for the energy consumed by the residential, industrial, commercial and other sectors. In other words, the PESI provides an indicator of the potential energetic self-sufficiency of each state. A PESI>1 (or a fulfillment of more than 100% of the *per capita* required energy) indicates an energy surplus in a state. This can be a valuable decision-making indicator, since states with a PESI>>1 may be able to produce energy for other contiguous states with a PESI<1.

2.6 Feedstock characterization

The elemental composition of the waste used in the simulations by state was assumed as the weighted average of the elemental composition of each type of residue generated in each state (Vassilev et al., 2010; Kumar et al., 2022; Silva et al., 2019), based on the average agricultural waste masses produced per state per year. The agricultural waste composition from different states throughout Mexico was collected from (SIAP, 2024); the information can be found in Table 5. A total of 13 different agricultural residues were considered, representing an estimated amount of 53 million tons per year, including maize, sugar cane, sorghum and wheat, among others. Information was not available for 5 out of the 31 states: Baja California, Campeche, Coahuila, Colima and Chiapas. The proximate analysis is not included since ashes do not participate in the reactions.

2.7 Cost analysis

To evaluate the cost of gasification, an Order-of-Magnitude estimate was made for each state. The base costs for Direct Capital Cost (DCI), utilities (water, electricity) consumption and other variable costs (for example, salaries) were adapted from (Boujjat et al., 2021) and are presented in Tables 6 and 7.

For the cost analysis, DCI, Fixed Costs (FC) and Variable Costs (VC) were considered. The DCI per state (DCI_{state}) was estimated scaling the base values in Table 6, deemed Direct Capital Cost base (DCI_{base}) and biomass capacity base (Bio_{base}); the biomass availability by state on dry basis (Bio_{state}) was considered and employed in Equation 28, updated to year 2024 using the Chemical Engineering Plant Cost Index (Boujjat et al., 2021). A moisture content of 20% in the residues was assumed for Bio_{state}; this cost does not include cost of land. Although conventional downstream processes in gasification systems, operations such as steam reforming, shift and Pressure Swing Absorption (PSA) are not part of the study, hence, are not considered in the economic analysis, thus reducing the DCI by 12%.

$$DCI_{state} = DCI_{base} \left(\frac{Bio_{state}}{Bio_{base}} \right)^{0.78} \tag{28}$$

For the estimation of fixed cost per state (FC_{state}), the labor cost (LC_{state}), the general and administrative expenses, estimated as 20% of the LC_{state} and the material maintenance costs and repairs, assumed to be equal to 0.5% of the project direct capital costs were considered (Boujjat et al., 2021). FC_{state} was estimated with Equation 29 (Boujjat et al., 2021):

$$FC_{state} = 1.2\, LC_{state} + 0.005\, DCI_{state} \tag{29}$$

LC_{state} was estimated by the Number of Operators (NO_{state}) and their salaries, according to Equation 30. NO_{state} was determined by scaling the plant staff base (NO_{base}) using Equation 31 (Boujjat et al., 2021). The Average Salary of Power

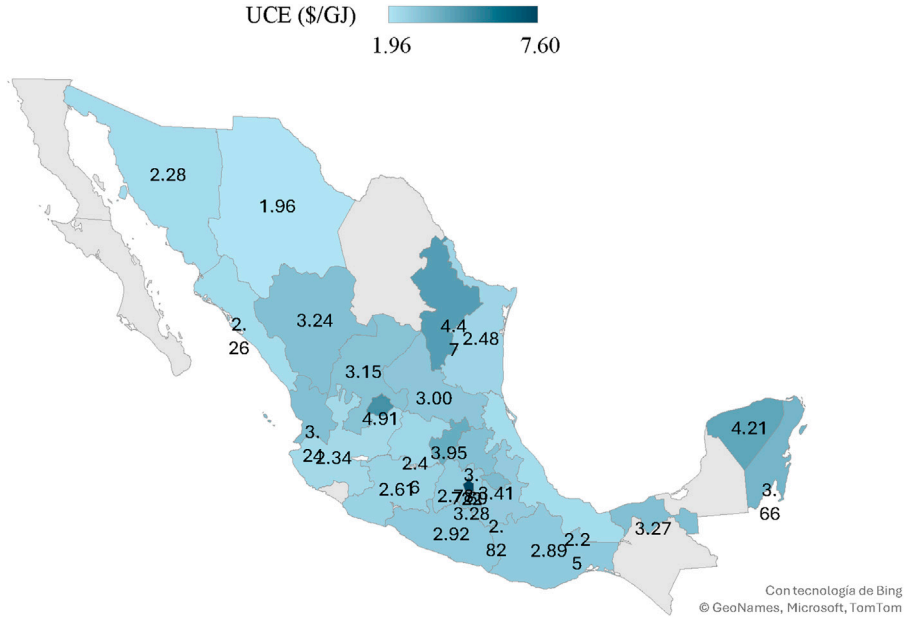

FIGURE 10
Unitary cost of energy per state (UCE_{state}).

Generation Machine Operators (ASO), presented in Table 6, was used in the estimation of LC_{state}.

$$LC_{state} = NO_{state}\, ASO \tag{30}$$

$$NO_{state} = NO_{base}\left(\frac{Bio_{state}}{Bio_{base}}\right)^{0.25} \tag{31}$$

Variable costs per state (VC_{state}) included electricity, water, biomass and other variable costs and were calculated using Equation 32.

$$VC_{state} = \left(WP_f Bio_{state} + WC_f E_{gasf}\right)W_p + \left(Ec_f E_p + Bio_p\right)Bio_{state} + OVC_{state} \tag{32}$$

Where WP_f, WC_f and Ec_f are water consumption factor for the gasification process, water consumption factor for mirror cleaning and electricity consumption factors, respectively; values are presented in Table 6. W_p, E_p and Bio_p are the prices of water, electricity and biomass, respectively, presented in Table 7; the prices were updated using producer price index reported by INEGI (INEGI, 2025). OVC_{state} represents Other Variable Costs per state and include other raw materials, waste treatment, solid waste disposal and environmental surcharges; these OVC_{state} were scaled from the base value (OVC_{base}) presented in Table 6 using Equation 33.

$$OVC_{state} = OVC_{base}\left(\frac{Bio_{state}}{Bio_{base}}\right)^{0.78} \tag{33}$$

The Total Variable Cost per state (TVC_{state}) was estimated by adding FC_{state} and VC_{state}. To estimate the Net Present Value of TVC_{state} ($NPTVC_{state}$), Equation 34 was used considering an inflation value of 4% (g), an interest rate of 12% (r) and 25 years of life of the plant (n).

$$NPTVC_{state} = TVC_{state}\,\frac{1-(1+g)^{n}(1+r)^{-n}}{r-g} \tag{34}$$

Then $NPTVC_{state}$ and DCI_{state} were added to estimate the Net Present Value of Cost per state (NPC_{state}). This value represents the total expenses of the project during its lifetime at present value and was used along with EDI calculated per state (EDI_{state}) to determine two indicators about the economic performance of the project. First indicator was the unitary cost per capacity of power production per state (UCC_{state}), according to Equation 35.

$$UCC_{state} = \frac{NPC_{state}}{33068.7\, EDI_{state}} \tag{35}$$

Where UCC_{state} is in $/kW of syngas produced, NPC_{state} is in $ and EDI_{state} in PJ/year. The factor 33068.7 was obtained considering 350 days/year and 24 h/d of operation.

The second indicator represents the unitary cost of energy per state (UCE_{state}) during the lifetime of the project and was obtained using Equation 36.

$$UCE_{state} = \frac{NPC_{state}}{1\text{x}10^{6}\, n\, EDI_{state}} \tag{36}$$

Where UCE_{state} is in $/GJ, NPC_{state} and EDI_{state} have the same units that in Equation 35.

3 Results and discussion

Simulations were conducted considering the maximum achievable temperature under the mean irradiation conditions for every state (Buentello-Montoya et al., 2023a). Air and (Mousavi Rabeti et al., 2023) steam as the gasification agent; although air gasification is an autothermal technology, the results are presented

since they can be useful to provide a comparison with steam gasification under the same conditions, considering that one of the bottlenecks for steam gasification lies in the energy required to produce steam at the given temperature (Buentello-Montoya et al., 2023a; Maytorena and Buentello-Montoya, 2022; Samani et al., 2024; Buentello-Montoya et al., 2023b). In the upcoming section, firstly the effect of the gasifying agent in the produced gas, and the process CCE and CGE is presented. Afterwards, the results are presented by state; in the "by state" analysis, the effect of the DNI, the biomass composition and biomass availability is assessed, where the effect in the energy production potential and the H_2/CO ratio is presented and discussed.

3.1 Effect of the gasifying agent in the syngas quality and process efficiency

The effect of the DNI in the produced gas LHV is shown in Figure 2, where the ER (for air gasification) was varied from 0.2 to 0.4 (usual for air gasification (Sikarwar et al., 2016)), while the SBR (for steam gasification) was varied from 0.5 to 1.0 (usual for steam gasification (Sikarwar et al., 2016)). Figure 2a corresponds to gasification using air, while Figure 2b portrays results from gasification using steam. It can be seen that in the case of air, the LHV increases with DNI (albeit slightly), whereas in the case of steam, the DNI results in a decrease in LHV. Higher DNI leads to higher temperatures, which favors the reverse WGS reaction thus decreasing the H_2 contents in the syngas. On the other hand, as expected (due to carbon and H_2 oxidation, as well as dilution of the gas with nitrogen) the LHV decreases with increasing ER and increases with the SBR (due to an increase in the hydrogen contents in the reactants).

With regards to the H_2/CO ratio, a significant difference can be seen when comparing the use of air and steam in gasification (Figure 3), where the ratio increases in a ratio of around 1:5 when changing air to steam. The increase occurs due to the abundance of H_2O for the WGS reaction, where the reaction occurs in reverse with increasing temperature due to its exothermicity. This implies that for the synthesis of products such as Fischer-Tropsch fuels, high temperatures (or alternatively, high DNIs) are not necessarily favorable. However, the DNI can be potentially controlled using window shade-like devices (Maytorena and Buentello-Montoya, 2024). With regards to the ER (in the case of air gasification), the ratio decreases with increasing ER (due to the production of additional CO from the carbon in the biomass). With respect to the SBR (for steam gasification), a marginal decrease occurs with increasing SBR due to shifts in equilibrium in the WGS and the Boudouard reactions (Buentello-Montoya et al., 2020). With air gasification, higher temperatures promote the decomposition of biomass to H_2, CO and CO_2. On the other hand, in the case of steam gasification, higher temperatures lead to the formation of large amounts of H_2O from H_2; this is further reflected when analyzing the H_2/CO ratio.

On the other hand, increasing the gasification temperature and ER (Figure 4a) results in an increased CCE. On the contrary, the CCE decreases with increasing SBR due to shifts in equilibrium in the Boudouard and the carbon gasification reactions (as portrayed in Figure 4b). At higher temperatures, higher CCEs are achieved using air than when compared to using steam. This can be attributed to thermodynamics favoring reactions such as combustion and the Boudouard reaction (Buentello-Montoya et al., 2020). On the other hand, the CGE increases with DNI using air (Figure 4c) and decreases with DNI using steam (Figure 4d). With regards to the mass of gasification agent, the increase in ER results in lower CGE (mainly due to dilution of the syngas with N_2) while the larger hydrogen availability with increasing SBR results in an increased LHV, leading to an increase in the CGE.

3.2 Energy density by state

Figure 5 provides information on the waste agricultural biomass availability by state, where 5a shows the average total produced biomass, Figure 5b shows the population by state, 5c shows the average produced biomass *per capita*, 5 days portrays a map of the normalized average biomass waste generation by state (calculated by diving the average production of state *i* by the average production of Sinaloa, the top producer) and 6e portrays the average yearly DNI by state. The produced biomass *per capita* was calculated using data available from Mexico's federal government (National Institute of Statistics and Geography Instituto Nacional de Estadística y Geografía, 2020). The largest mass of residues is located in the states of Sinaloa, Jalisco and Veracruz, while the largest average generation of residues *per capita* can be found in the states of Sinaloa, Tamaulipas and Sonora. Regarding sun energy availability, the states with the largest average DNI are Chihuahua, Sonora and Durango. This shows that there is no correspondence between the availability of residues and irradiation.

Figure 6a presents the EDI calculated per state via gasification with air, while Figure 6b shows the EDI of gasification with steam. The presented results were obtained with a constant gasification agent mass to achieve a gas yield of ≈1.2 Nm^3/kg biomass (ER of 0.2, for air and SBR of 0.5 for steam).

The states with the highest EDIs using air are Sinaloa, Chihuahua, Jalisco and Veracruz, with 60, 55.9, 46.6 and 42.5 PJ/year, respectively. Interestingly, although the EDI tends to be higher in the north, the relationship does not hold true for every case. Using steam as a gasifying agent results in Sinaloa, Veracruz, Chihuahua and Jalisco, with 126.8, 101.7, 100.1 and 98.7 PJ/year, respectively, being the states with the highest values. In contrast, for both gasifying agents, Ciudad de México, Aguascalientes, Nuevo León, Yucatán and Querétaro result in the lowest energy potential, where 0.10, 0.65, 1.1, 1.4 years 2.1 PJ/year were obtained with air, and 0.24, 1.3, 2.6, 3.3 and 4.5 PJ/year were obtained with steam. The results indicate that (1) the states with the most and least potential are the same, regardless of the gasification agent, and (Mousavi Rabeti et al., 2023) the defining aspect in the potential for solar gasification as a source of energy is the biomass availability, above the biomass composition and the DNI. This goes in agreement with Machine-Learning studies that report that the LHV of a syngas is more than anything affected by the gasification temperature, even if the H_2 content in the syngas is directly related to the hydrogen contents in the biomasses, while the biomass component with the highest importance in the overall process performance is carbon (Buentello-Montoya et al., 2025). Notwithstanding, the biomass composition has a significant effect. For example, Chihuahua ranks fourth in waste generation (Figure 6a) but ranks second in

the EDI using air, and Veracruz ranks third in waste generation, but ranks second in EDI with steam. Generally speaking, the energy density using steam increases by a factor of around 2.2 when replacing air with steam. This highlights the potential of the inclusion of solar energy for the allothermal process.

3.3 H_2/CO by state

H_2/CO is an important indicator of the potential applications of syngas, as, for example, for the synthesis of some chemicals a high H_2/CO ratio (>2) is necessary. Figure 7 shows the H_2/CO by state, where Figures 7a,b represent the use of air and steam as gasification agent, respectively. By comparing Figure 7 with Figure 5e, it can be inferred that a negative relationship between the DNI and the H_2/CO exists, where the increase in DNI has a more significant effect when using steam; the more significant effect can be related to the exothermicity of the water-gas shift reaction. Still, when using steam, most states have a H_2/CO>>2, indicating a potential for additional syngas applications besides energy. However, from the biomass availability (Figure 5), it can be inferred the states with the highest H_2/CO ratio (Veracruz with 26.7, Tamaulipas with 11.2 and Nuevo Leon with 12.8, all located in eastern Mexico) also have a low-to-average normalized biomass productions (Veracruz 0.77, Tamaulipas 0.54 and Nuevo Leon 0.02), indicating that in Mexico, the H_2/CO is not the sole important decision making indicator for a H_2-based chemicals plant, since this criteria may result in feedstock availability problem. Additionally, something to notice is that the states with higher H_2/CO ratio are close to existing petrochemical facilities (in Guanajuato, Hidalgo Tabasco and Veracruz), which can be an opportunity to use that infrastructure to convert the syngas into chemicals through processes such as Fischer-Tropsch (Gobierno de México, 2022). Moreover, establishing a plant for biomass processing in the states by the Gulf of Mexico (Veracruz and Tabasco) could benefit from other economic activities such as aquaculture, or from waste such as algae washed ashore; this analysis is outside of the scope of the present work, however.

3.4 Per capita self-sufficiency index

To evaluate the extent to which each state could rely on its own agricultural residues and solar resource for energy generation, the Per Capita Energy Self-Sufficiency Index (PESI), defined in Equation 27, was employed. The PESI compares the theoretical energy content of syngas produced from the waste biomass produced *per capita* to the average *per capita* energy consumption in Mexico, which is approximately 2,425 kWh/year (Secretaría de Energía SENER, 2023). A PESI value greater than 1 indicates that a state could theoretically generate enough energy from solar gasification of agricultural biomass waste to exceed its own demand, whereas values below 1 indicate that local residues are insufficient, and that external energy sources or complementary technologies would be required. By analyzing the results in terms of PESI, it becomes possible to determine which states have potential for energy self-sufficiency, those that might benefit from regional integration, and that where solar gasification may be unsuitable.

Figure 8 shows bar plots of the PESI using (Figure 8a) air and (Figure 8b) steam as gasification agents, while Figures 8c,d show a map of the geographical distribution of the PESI using air and steam, respectively. Finally, Figures 8e,f portray the PESI for both gasification agents as a function of the available waste biomass and the DNI.

From the results found in Figure 8, the states can be grouped into three categories.

1. Exceeded PESI (PESI≥ 100%), where the energy potential surpasses the *per capita* consumption. These states are suitable for solar gasification, and may benefit from not only energy generation, but the production of compounds such as ammonia from the produced hydrogen:
   - Using air: Sinaloa (236%), Sonora (132%), Chihuahua (120%) and Tamaulipas (100%).
   - Using steam: Sinaloa (480%), Sonora (245%), Tamaulipas (222%), Chihuahua (209%), Nayarit (154%), Veracruz (144%), Jalisco (135%), Guanajuato (127%) and Michoacán (124%).
2. Moderate PESI (50%<PESI<100%), which may include states with a significant energy production potential, but due to population, may not satisfy the required energy and thus may require synergy from other technologies or support from adjacent states. These states may be suitable for a solar gasification plant:
   - Using air: Nayarit (74%) and Michoacán (58%).
   - Using steam: Zacatecas (93%) and Tabasco (53%).
3. Low PESI (PESI<50%), where the potential for energy production is low compared to its requirements, due to limitations in the available waste biomass, and therefore, may be questionable for solar gasification unless supported with other technologies:
   - Using air: Zacatecas (48%) and Ciudad de México (0.14%).
   - Using steam: Quintana Roo (45%) a Ciudad de México (0.31%).

From the results and based on the geographical distribution and on the categories, different actions can be undertaken.

1. Exceeded PESI: The surplus energy could be exported however attention must be paid to the energy consumed (and the associated carbon footprint) during transportation and the associated logistics. Additionally, hydrogen-based refineries and processes can be established to produce chemicals such as methane, methanol or urea (Masjedi et al., 2024; Sinha and Panigrahy, 2024; Alfian and Purwanto, 2019).

Moderate PESI: Moderate PESI states may benefit from solar gasification but will be hardly able to rely on it as the sole source of energy, therefore, are recommended to potentially work in tandem with Exceeded PESI states to satisfy their needs.

2. Low PESI: Low PESI states may benefit more from other technologies such as biodigesters.

Remarkably, a high PESI value does not necessarily mean that the state is suitable for solar gasification, since interest might be in the production of chemicals which require parameters such as a large H_2/CO ratio. Moreover, states with a PESI value can be either a hub for chemical production or energy production, to satisfy the demands of other states. For example, Sinaloa (PESI of 2.36 with air and 4.80 with steam) could provide contiguous states with low PESIs (0.60 for steam and 0.32 for air) with chemicals and energy.

With regards to the relationship between the available waste biomass (Figures 8e,f), the DNI and the PESI, it can be seen that the main contributor to the PESI is the available waste biomass. Therefore, the potential use (e.g., as a fuel, or for downstream processing) of the produced syngas can be attributed to the DNI and the average biomass composition, whereas states with a large amount of available agricultural biomass are suitable for energy production.

Regarding the geographical distribution and its relationship with PESI and energy availability, Veracruz is connected to the center of Mexico, where no state has a PESI score larger than 1, and where more than 30% of the overall population (and energy consumption) is found, making it prospect for a solar gasification plant.

3.5 Economic indicators

To evaluate the economic performance of the process, UCC_{state} and UCE_{state} where estimated and used as indicators. Figure 9 presents the behavior of UCC_{state}. This indicator shows that smaller production capacity (i.e., states with lower biomass production) leads to higher costs, which is expected because of economy of scale. At the same time, a large decrease in the UCC_{state} can be observed for capacities below 2 million tons of biomass processed per year. With production above 1.9 million tons/year, the reduction in cost is less pronounced, varying around 18% with a variation of 5 million tons/year in plan capacity. The range between 1,700–2,100 $/kW is larger than those reported in literature (Lourinho et al., 2023), which varies between 675–1,300 $/kW; the reported values do not include all the variable costs considered in this work, however.

Figure 10 presents the values of UCE_{state}, where Chihuahua has the smallest value with 1.96 $/GJ, followed by Sinaloa, Veracruz and Sonora, with 2.25, 2.26 and 2.28 $/GJ respectively. These results show that the cost of production of syngas can be competitive with prices of natural gas in México, which have varied between 2.97 and 6.79 $/GJ during the period of 2020–2024 (Secretaría de Energía SENER, 2023).

3.6 Overview of environmental benefits of the technology

The proposed technology can potentially decrease the environmental burden associated to satisfying the country's energy needs. With respect to land use, the proposed systems relies on existing agricultural and municipal residues as feedstock, rather than dedicated energy crops (first generation biofuels). This reduces pressure on fertile land and avoids negative impacts associated with land-use change (Parthasarathy et al., 2022). It is worth noting that most of these residues are currently disposed of in open-air landfills in Mexico, since this is the most economical and straightforward option; however, such disposal is associated to environmental and health problems due to potential emissions, infiltration of pollutants to groundwater bodies, and particle matter associated to health hazards (Foong et al., 2020). On the other hand, regarding water consumption, solar thermochemical systems generally require less water than conventional plants whose energy is supplied by combustion since do not rely on steam cycles, given that the primary energy input for solar gasification plants is solar radiation coupled with locally available biomass, in addition that no additional water is required to harvest the crops (Eldredge, 2021). In terms of greenhouse gas emissions, solar gasification avoids the use of heat derived from fossil fuels or from the direct burning of biomass, significantly reducing the carbon footprint and greenhouse gas emissions (Maytorena and Buentello-Montoya, 2024; Eldredge, 2021; Nzihou et al., 2012). In addition, the co-production of biochar provides complementary benefits, as this material enables carbon capture and storage while improving soil physical properties such as aeration, workability, and water retention capacity (Parthasarathy et al., 2022), associated to the recognition of biochar as an advanced and sustainable material with the potential to increase soil fertility, improve crop yields, and sequester atmospheric carbon (Qambrani et al., 2017). All in all, have the potential to reduce emissions associated to energy production while fostering circular economy strategies based on waste utilization, to produce valuable chemicals such as Fischer-Tropsch liquids (Li et al., 2017). Nevertheless, it must be acknowledged that a full-fledged life cycle assessment (LCA) is necessary to comprehensively quantify these benefits and impacts. Although such an analysis is beyond the scope of the present work, it is proposed as a future research direction to more fully evaluate the environmental implications of this technology.

4 Summary and conclusions

An analysis of the potential of solar gasification in Mexico was conducted using Gibbs free energy minimization-based simulations to assess the potential of steam-based solar gasification. Air and steam were compared as gasifying agents using average direct normal irradiation to heat the reactor. Results demonstrate that although the syngas quality (in terms of the Lower Heating Value and H_2/CO ratio) is affected by direct normal irradiance (where higher irradiation tends to decrease the lower heating value and H_2/CO ratio of the produced syngas), the decisive factors for solar gasification as a source of energy are the biomass availability and composition, rather than the solar resource. Moreover, it was found that steam produces better quality syngas than air, highlighting the necessity to find energy sources for steam gasification. A Per Capita Energy Self-Sufficiency Index (PESI) was computed, which shows that states with abundant agricultural residues, such as Sinaloa and Veracruz, could meet or even surpass their local energy demand through solar gasification. Moreover, the economic analysis shows that states with high biomass and energy production can have potential for gasification, since the unitary cost of energy of around 2–2.3

$/GJ is competitive with natural gas, whose cost in Mexico varies between 2.97–6.79 $/GJ.

Overall, the findings highlight solar biomass gasification as a promising strategy for coupling Mexico's agricultural waste streams with the abundance of solar resources, potentially contributing to decentralized energy supply and to the development of hydrogen-based chemical industries. Future research should extend this analysis by considering seasonal feedstock variability, logistics and supply chain aspects, and the environmental footprint of large-scale implementation. Moreover, a deeper economic analysis focused on the states of Sinaloa, Veracruz and Chihuahua (and possibly Jalisco) may be worthwhile, considering specifics of each state such as land price, loans, taxes, variation in salaries, biomass and utilities costs and energy sale prices.

Data availability statement

The datasets presented in this article are not readily available because The data is confidential, unfortunately. Requests to access the datasets should be directed to David Buentello-Montoya, david.buentello@tec.mx.

Author contributions

VM-S: Conceptualization, Formal Analysis, Investigation, Methodology, Writing – original draft, Writing – review and editing. DB-M: Conceptualization, Investigation, Methodology, Software, Supervision, Validation, Writing – original draft, Writing – review and editing. HA: Data curation, Formal Analysis, Funding acquisition, Investigation, Methodology, Project administration, Writing – original draft, Writing – review and editing.

Funding

The authors declare that financial support was received for the research and/or publication of this article. This work was supported by the Instituto Tecnológico y de Estudios Superiores de Monterrey through the Publications Support Fund (FAP, by its initials in Spanish).

Conflict of interest

The authors declare that the research was conducted in the absence of any commercial or financial relationships that could be construed as a potential conflict of interest.

Generative AI statement

The authors declare that no Generative AI was used in the creation of this manuscript.

Any alternative text (alt text) provided alongside figures in this article has been generated by Frontiers with the support of artificial intelligence and reasonable efforts have been made to ensure accuracy, including review by the authors wherever possible. If you identify any issues, please contact us.

Publisher's note

References

Abanades, S., Rodat, S., and Boujjat, H. (2021). Solar thermochemical green fuels production: a review of biomass pyro-gasification, solar reactor concepts and modelling methods. *Energies (Basel)* 14 (5), 1494. doi:10.3390/en14051494

Aldana, H., Lozano, F. J., and Acevedo, J. (2014). Evaluating the potential for producing energy from agricultural residues in México using MILP optimization. *Biomass Bioenergy* 67, 372–389. doi:10.1016/j.biombioe.2014.05.022

Alfian, M., and Purwanto, W. W. (2019). Multi-objective optimization of green urea production. *Energy Sci. Eng.* 7 (2), 292–304. doi:10.1002/ese3.281

Arribas, L., Arconada, N., González-Fernández, C., Löhrl, C., González-Aguilar, J., Kaltschmitt, M., et al. (2017). Solar-driven pyrolysis and gasification of low-grade carbonaceous materials. *Int. J. Hydrogen Energy* 42 (19), 13598–13606. doi:10.1016/j.ijhydene.2017.02.026

Boujjat, H., Rodat, S., Chuayboon, S., and Abanades, S. (2020). Experimental and CFD investigation of inert bed materials effects in a high-temperature conical cavity-type reactor for continuous solar-driven steam gasification of biomass. *Chem. Eng. Sci.*, 228. doi:10.1016/j.ces.2020.115970

Boujjat, H., Rodat, S., and Abanades, S. (2021). Techno-economic assessment of solar-driven steam gasification of biomass for large-scale hydrogen production. *Processes* 9 (3), 462. doi:10.3390/pr9030462

Buentello-Montoya, D., Zhang, X., Li, J., Ranade, V., Marques, S., and Geron, M. (2020). Performance of biochar as a catalyst for tar steam reforming: effect of the porous structure. *Appl. Energy* 259, 114176. doi:10.1016/j.apenergy.2019.114176

Buentello-Montoya, D. A., Armenta-Gutiérrez, M. Á., and Maytorena-Soria, V. M. (2023a). Parametric modelling study to determine the feasibility of the Co-Gasification of macroalgae and plastics for the production of hydrogen-rich syngas. *Energies (Basel)* 16 (19), 6819. doi:10.3390/en16196819

Buentello-Montoya, D. A., Duarte-Ruiz, C. A., and Maldonado-Escalante, J. F. (2023b). Co-gasification of waste PET, PP and biomass for energy recovery: a thermodynamic model to assess the produced syngas quality. *Energy*, 266. doi:10.1016/j.energy.2022.126510

Buentello-Montoya, D. A., and Maytorena-Soria, V. M. (2025). Feature importance analysis of solar gasification of biomass via machine learning models. *Energies (Basel).* 18 (16), 4409. doi:10.3390/en18164409

Cho, M. H., Mun, T. Y., Choi, Y. K., and Kim, J. S. (2014). Two-stage air gasification of mixed plastic waste: olivine as the bed material and effects of various additives and a nickel-plated distributor on the tar removal. *Energy* 70, 128–134. doi:10.1016/j.energy.2014.03.097

Curcio, A., Rodat, S., Vuillerme, V., and Abanades, S. (2021). Experimental assessment of woody biomass gasification in a hybridized solar powered reactor featuring direct and indirect heating modes. *Int. J. Hydrogen Energy* 46 (75), 37192–37207. doi:10.1016/j.ijhydene.2021.09.008

Duan, W., Yu, Q., Xie, H., Qin, Q., and Zuo, Z. (2014). Thermodynamic analysis of hydrogen-rich gas generation from coal/steam gasification using blast furnace slag as heat carrier. *Int. J. Hydrogen Energy* 39 (22), 11611–11619. doi:10.1016/j.ijhydene.2014.05.125

El Sol de Hidalgo (2025). *Valle del Mezquital: Forage Bales Reach 160 Pesos for Sale*. Pachuca, Hidalgo: El Sol de Hidalgo. Available online at: https://oem.com.mx/elsoldehidalgo/local/valle-del-mezquital-pacas-de-forraje-alcanzan-los-160-pesos-a-la-venta-13555882.

Eldredge, T. V. (2021). The feasibility of solar assisted pyrolysis of sewer sludge and its potential for CO2 emissions reductions. *Energy* 226, 120296. doi:10.1016/j.energy.2021.120296

Fazil, A., Kumar, S., and Mahajani, S. M. (2022). Downdraft co-gasification of high ash biomass and plastics. *Energy*, 243. doi:10.1016/j.energy.2021.123055

Foong, S. Y., Liew, R. K., Yang, Y., Cheng, Y. W., Yek, P. N. Y., Wan Mahari, W. A., et al. (2020). Valorization of biomass waste to engineered activated biochar by microwave pyrolysis: progress, challenges, and future directions. *Chem. Eng. J.* 389, 124401. doi:10.1016/j.cej.2020.124401

Freda, C., Tarquini, P., Sharma, V. K., and Braccio, G. (2022). Thermodynamic improvement of solar driven gasification compared to conventional one. *Energy*, 261. doi:10.1016/j.energy.2022.124953

Frenklach, M. (2002). Reaction mechanism of soot formation in flames. *Phys. Chem. Chem. Phys.* 4 (11), 2028–2037. doi:10.1039/b110045a

Gai, C., and Dong, Y. (2012). Experimental study on non-woody biomass gasification in a downdraft gasifier. *Int. J. Hydrogen Energy* 37 (6), 4935–4944. doi:10.1016/j.ijhydene.2011.12.031

Global Solar Atlas (2020). *Global Solar Atlas*. Sonora, Mexico: Global Solar Atlas. Available online at: https://globalsolaratlas.info/detail?c=28.971803,-110.99762,11&s=29.098177,-110.954361&m=site.

Gobierno de México (2022). *Refinación*. Estado de Mexico: Gobierno de Mexico.

Hathaway, B. J., and Davidson, J. H. (2017). Demonstration of a prototype molten salt solar gasification reactor. *Sol. Energy* 142, 224–230. doi:10.1016/j.solener.2016.12.032

Hathaway, B. J., and Davidson, J. H. (2021). Autothermal hybridization and controlled production of hydrogen-rich syngas in a molten salt solar gasifier. *Int. J. Hydrogen Energy* 46 (29), 15257–15267. doi:10.1016/j.ijhydene.2021.02.048

INEGI (2025). *Indicator Bank. National Institute of Statistics and Geography*. Aguascalientes: INEGI. Available online at: https://www.inegi.org.mx/app/indicadores/?tm=0&t=100005000032#D100005000032#D910491_100005000032

Jayah, T. H., Aye, L., Fuller, R. J., and Stewart, D. F. (2003). Computer simulation of a downdraft wood gasifier for tea drying. *Biomass Bioenergy* 25 (4), 459–469. doi:10.1016/s0961-9534(03)00037-0

Jess, A. (1996). Mechanisms and kinetics of thermal reactions of aromatic hydrocarbons from pyrolysis of solid fuels. *Fuel* 75 (12), 1441–1448. doi:10.1016/0016-2361(96)00136-6

Khartchenko, N., and Kharchenko, V. (2014). *Advanced energy systems*. Second edition. New York, NY: Taylor and Francis Group.

Kodama, T., Gokon, N., Enomoto, S. I., Itoh, S., and Hatamachi, T. (2010). Coal coke gasification in a windowed solar chemical reactor for beam-down optics. *J. Sol. Energy Eng. Trans. ASME.* 132 (4), 041004. doi:10.1115/1.4002081

Kramb, J., Konttinen, J., Gómez-barea, A., Moilanen, A., and Umeki, K. (2014). Modeling biomass char gasification kinetics for improving prediction of carbon conversion in a fluidized bed gasifier. *FUEL* 132, 107–115. doi:10.1016/j.fuel.2014.04.014

Kumar, V. A., Singh, S., Kumar Rathore, A., Singh Thakur, L., Shankar, R., and Mondal, P. (2022). Investigation of kinetic and thermodynamic parameters for pyrolysis of peanut shell using thermogravimetric analysis. *Biomass Convers. Biorefin* 31. doi:10.1007/s13399-020-00972-y

Li, P., Sadhwani, N., Yuan, Z., and Eden, M. R. (2017). Process simulation and economic analysis of producing liquid transportation fuels from biomass. *Comput. Aided Chem. Eng.* 40, 2515–2520. doi:10.1016/b978-0-444-63965-3.50421-9

Li, J., Qiao, Y., Chen, X., Zong, P., Qin, S., Wu, Y., et al. (2019). Steam gasification of land, coastal zone and marine biomass by thermal gravimetric analyzer and a free-fall tubular gasifier: biochars reactivity and hydrogen-rich syngas production. *Bioresour. Technol.* 289 (May), 121495. doi:10.1016/j.biortech.2019.121495

Li, X., Shen, Y., Wei, L., He, C., Lapkin, A. A., Lipiński, W., et al. (2020). Hydrogen production of solar-driven steam gasification of sewage sludge in an indirectly irradiated fluidized-bed reactor. *Appl. Energy* 261, 114229. doi:10.1016/j.apenergy.2019.114229

Li, X., Chen, J., Hu, Q., Chu, P., Dai, Y., and Wang, C. H. (2021). Solar-driven gasification in an indirectly-irradiated thermochemical reactor with a clapboard-type internally-circulating fluidized bed. *Energy Convers. Manag.* 248, 114795. doi:10.1016/j.enconman.2021.114795

Loha, C., Chatterjee, P. K., and Chattopadhyay, H. (2011). Performance of fluidized bed steam gasification of biomass - modeling and experiment. *Energy Convers. Manag.* 52 (3), 1583–1588. doi:10.1016/j.enconman.2010.11.003

Lourinho, G., Alves, O., Garcia, B., Rijo, B., Brito, P., and Nobre, C. (2023). Costs of gasification technologies for energy and fuel production: overview, analysis, and numerical estimation. *Recycling* 8 (3), 49. doi:10.3390/recycling8030049

Loutzenhiser, P. G., and Muroyama, A. P. (2017). A review of the state-of-the-art in solar-driven gasification processes with carbonaceous materials. *Sol. Energy* 156, 93–100. doi:10.1016/j.solener.2017.05.008

Masjedi, S. K., Kazemi, A., Moeinnadini, M., Khaki, E., and Olsen, S. I. (2024). Urea production: an absolute environmental sustainability assessment. *Sci. Total Environ.*, 908. doi:10.1016/j.scitotenv.2023.168225

Maytorena, V. M., and Buentello-Montoya, D. A. (2022). Multiphase simulation and parametric study of direct vapor generation for a solar organic rankine cycle. *Appl. Therm. Eng.*, 216. doi:10.1016/j.applthermaleng.2022.119096

Maytorena, V. M., and Buentello-Montoya, D. A. (2024). Worldwide developments and challenges for solar pyrolysis. *Heliyon*, 10, e35464. doi:10.1016/j.heliyon.2024.e35464

Mexican Institute for Competitiveness (IMCO) (2023). *The real cost of water in Mexico: an analysis of tariffs and their impacts on society*. Miguel Hidalgo: Mexican Institute for Competitiveness.

Ministry of Economy (Secretaría de Economía) (2025). *Operators of Machines for Power Generation*. Mexico: Ministry of Economy. Available online at: https://www.economia.gob.mx/datamexico/es/profile/occupation/operadores-de-maquinas-para-la-generacion-de-energia.

Molina-Guerrero, C. E., Sanchez, A., and Vázquez-Núñez, E. (2020). Energy potential of agricultural residues generated in Mexico and their use for butanol and electricity production under a biorefinery configuration. *Environ. Sci. Pollut. Res.* 27 (23), 28607–28622. doi:10.1007/s11356-020-08430-y

Mousavi Rabeti, S. A., Khoshgoftar Manesh, M. H., and Amidpour, M. (2023). Techno-economic and environmental assessment of a novel polygeneration system based on integration of biomass air-steam gasification and solar parabolic trough collector. *Sustain. Energy Technol. Assessments* 56, 103030. doi:10.1016/j.seta.2023.103030

Müller, F., Poživil, P., van Eyk, P. J., Villarrazo, A., Haueter, P., Wieckert, C., et al. (2017). A pressurized high-flux solar reactor for the efficient thermochemical gasification of carbonaceous feedstock. *Fuel* 193, 432–443. doi:10.1016/j.fuel.2016.12.036

Muroyama, A. P., Guscetti, I., Schieber, G. L., Haussener, S., and Loutzenhiser, P. G. (2018). Design and demonstration of a prototype 1.5 kWth hybrid solar/autothermal steam gasifier. *Fuel* 211, 331–340. doi:10.1016/j.fuel.2017.09.059

Nathan, G. J., Dally, B. B., Alwahabi, Z. T., Van Eyk, P. J., Jafarian, M., and Ashman, P. J. (2017). Research challenges in combustion and gasification arising from emerging technologies employing directly irradiated concentrating solar thermal radiation. *Proc. Combust. Inst.* 36 (2), 2055–2074. doi:10.1016/j.proci.2016.07.044

National Institute of Statistics and Geography (Instituto Nacional de Estadística y Geografía) (2020). *Cuéntame México*. Aguascaliente: National Institute of Statistics and Geography.

Norinaga, K., Yang, H., Tanaka, R., Appari, S., Iwanaga, K., Takashima, Y., et al. (2014). A mechanistic study on the reaction pathways leading to benzene and naphthalene in cellulose vapor phase cracking. *Biomass Bioenergy* 69, 144–154. doi:10.1016/j.biombioe.2014.07.008

Nzihou, A., Flamant, G., and Stanmore, B. (2012). Synthetic fuels from biomass using concentrated solar energy – a review. *Energy* 42 (1), 121–131. doi:10.1016/j.energy.2012.03.077

Parthasarathy, P., Al-Ansari, T., Mackey, H. R., Sheeba Narayanan, K., and McKay, G. (2022). A review on prominent animal and municipal wastes as potential feedstocks for solar pyrolysis for biochar production. *Fuel* 15, 316. doi:10.1016/j.fuel.2022.123378

Pecchi, M., and Baratieri, M. (2019). Coupling anaerobic digestion with gasification, pyrolysis or hydrothermal carbonization: a review. *Renew. Sustain. Energy Rev.* 105, 462–475. doi:10.1016/j.rser.2019.02.003

Privat, R., Jaubert, J. N., Berger, E., Coniglio, L., Lemaitre, C., Meimaroglou, D., et al. (2016). Teaching the concept of gibbs energy minimization through its application to phase-equilibrium calculation. *J. Chem. Educ.* 93 (9), 1569–1577. doi:10.1021/acs.jchemed.6b00205

Puig-Arnavat, M., Bruno, J. C., and Coronas, A. (2010). Review and analysis of biomass gasification models. *Renew. Sustain. Energy Rev.* 14 (9), 2841–2851. doi:10.1016/j.rser.2010.07.030

Qambrani, N. A., Rahman, M. M., Won, S., Shim, S., and Ra, C. (2017). Biochar properties and eco-friendly applications for climate change mitigation, waste management, and wastewater treatment: a review. *Renew. Sustain. Energy Rev.* 79, 255–273. doi:10.1016/j.rser.2017.05.057

Rafati, M., Wang, L., Dayton, D. C., Schimmel, K., Kabadi, V., and Shahbazi, A. (2017). Techno-economic analysis of production of fischer-tropsch liquids *via* biomass gasification: the effects of fischer-tropsch catalysts and natural gas co-feeding. *Energy Convers. Manag.* 133, 153–166. doi:10.1016/j.enconman.2016.11.051

Sajjadnejad, M., Haghshenas, S. M. S., Targhi, V. T., Zahmatkesh, H. G., and Naeimi, M. (2020). Utilization of sustainable energies for purification of water. *Adv. J. Chem. Sect. A. Sami Publ. Co.* 3, 493–509. doi:10.33945/SAMI/AJCA.2020.4.11

Samani, N., Khalil, R., Seljeskog, M., Bakken, J., Thapa, R. K., and Eikeland, M. S. (2024). Experimental and simulation studies of oxygen-blown, steam-injected, entrained flow gasification of lignin. *Fuel* 15, 362. doi:10.1016/j.fuel.2023.130713

Secretaría de Energía (SENER) (2023). *Programa de Desarrollo del Sistema Eléctrico Nacional*. Mexico: Secretaría de Energía.

SIAP (2024). *Sistema de información Agroalimentaria de Consulta. Módulo agrícola estatal*.

Sikarwar, V. S., Zhao, M., Clough, P., Yao, J., Zhong, X., Memon, M. Z., et al. (2016). An overview of advances in biomass gasification. *Energy Environ. Sci.* 9 (10), 2939–2977. doi:10.1039/c6ee00935b

Silva, J. E., Calixto, G. Q., de Almeida, C. C., Melo, D. M. A., Melo, M. A. F., Freitas, J. C. O., et al. (2019). Energy potential and thermogravimetric study of pyrolysis kinetics of biomass wastes. *J. Therm. Anal. Calorim.* 137 (5), 1635–1643. doi:10.1007/s10973-019-08048-4

Sinha, M., and Panigrahy, S. R. (2024). Unveiling the urea market of the American continent. *J. Exp. Agric. Int.* 46 (1), 129–136. doi:10.9734/jeai/2024/v46i12302

Tuomi, S., Kaisalo, N., Simell, P., and Kurkela, E. (2015). Effect of pressure on tar decomposition activity of different bed materials in biomass gasification conditions. *Fuel* 158, 293–305. doi:10.1016/j.fuel.2015.05.051

Vassilev, S. V., Baxter, D., Andersen, L. K., and Vassileva, C. G. (2010). An overview of the chemical composition of biomass. *Fuel* 89 (5), 913–933. doi:10.1016/j.fuel.2009.10.022

Wieckert, C., Obrist, A., Zedtwitz, P., Maag, G., and Steinfeld, A. (2013). Syngas production by thermochemical gasification of carbonaceous waste materials in a 150 kW_{th} packed-bed solar reactor. *Energy and Fuels* 27 (8), 4770–4776. doi:10.1021/ef4008399

World Bank (2020). *Solar photovoltaic power potential by country*. Washington, DC: World Bank.

Xiao, R., Jin, B., Zhou, H., Zhong, Z., and Zhang, M. (2007). Air gasification of polypropylene plastic waste in fluidized bed gasifier. *Energy Convers. Manag.* 48 (3), 778–786. doi:10.1016/j.enconman.2006.09.004